lubricants

MDPI

Article

Understanding the Influences of Multiscale Waviness on the Elastohydrodynamic Lubrication Performance, Part II: The Partial-Film Condition

Yuechang Wang [1] and Ying Liu [2,*]

[1] School of Mechanical Engineering and Automation, Harbin Institute of Technology, Shenzhen 518055, China; wangyuechang@hit.edu.cn
[2] State Key Laboratory of Tribology in Advanced Equipment, Tsinghua University, Beijing 100084, China
* Correspondence: liuying@mail.tsinghua.edu.cn

Abstract: This paper is the second part of a two-part report studying the responses of a typical point-contact elastohydrodynamic lubrication (EHL) system to multiscale roughness mimicked by wavy surfaces. The wavy surfaces are defined by three key parameters: amplitudes, frequencies, and directions. The previous Part I paper focuses on the full film lubrication condition, while the current paper focuses on the partial film regime where asperity contacts occur. A transient thermal EHL model simulates lubrication problems with different waviness parameters, loads, and speeds. The total number of simulations is 1600. Performance parameters, including the asperity contact ratio, minimum film thickness, maximum pressure, central point film thickness, central point pressure, mean film thickness, coefficient of friction (COF), and the maximum temperature rise, are obtained for each simulation. These performance parameters are post-processed in the same manner as those in the previous Part I paper. The influences of the waviness parameters, load, and speed values on the eight performance parameters are discussed.

Keywords: thermal elastohydrodynamic lubrication; partial film; multiscale waviness

Citation: Wang, Y.; Liu, Y. Understanding the Influences of Multiscale Waviness on the Elastohydrodynamic Lubrication Performance, Part II: The Partial-Film Condition. *Lubricants* **2024**, *12*, 190. https://doi.org/10.3390/lubricants12060190

Received: 22 April 2024
Revised: 22 May 2024
Accepted: 27 May 2024
Published: 28 May 2024

1. Introduction

In the previous Part I paper [1], the background and significance of this series of works were thoroughly explained. Regarding the completeness of the current paper, the whole story is briefly repeated here.

In most cases, modeling realistic tribology systems requires surface roughness as a crucial input variable [2]. Realistic representation of the roughness is the foundation of such modeling processes. However, the multiscale nature of roughness, which has drawn the attention of researchers since the work of Archard in 1957 [3], makes it hard to clarify the question: how to identify the appropriate scales of roughness relevant to specific tribology systems?

Finding the answers to this question has at least three significant advantages for the tribology community. The first advantage is saving computational resources by modeling tribology systems within the roughness scales that most relate to them. The second one helps the industry reduce costs and increase efficiency by measuring the surface topography of parts on the relevant scales. The third one is improving tribological performance by designing multiscale roughness.

The question above has been studied by more and more researchers in recent years. Currently, two kinds of strategies are used to solve the question of how to characterize roughness.

The first category uses the nonstationary random process to describe the multiscale roughness features [4]. Then, in the 1980s, fractal concepts developed rapidly [5]. As fractal methods show great potential in characterizing the multiscale features by scale-invariant

parameters, they were soon used to describe the nonstationary roughness [6]. Then, fractal roughness is successfully used to boost the studies of rough contact mechanics [7–10]. Researchers found that the roughness scales have disparate effects on different contact quantities. For example, high-frequency components of rough surfaces affect the real contact area and rubber friction dissipation more [11]. In contrast, low-frequency components influence stiffness and electrical conductance more [12,13].

The other category uses the stationary random process to describe roughness. This method started with Longuet–Higgins [14] and Nayak [15]. They build the fundamentals of the modern roughness characterization parameters that are widely used. Compared to nonstationary or fractal roughness characterized by an analytical equation, stationary roughness can be determined by two functions: height probability density (HPD) and power spectral density (PSD). Thus, stationary roughness is much easier to generate numerically. The outcome is a discrete roughness height matrix, which is more popular with modeling lubrication systems. For example, the pioneering work of Patir and Cheng [16–18] and the unified Reynolds equation of Hu and Zhu [19–28] need roughness height matrix data as an essential input variable. However, previous studies, such as Demirci et al. [22] and Zhang et al. [26], only showed that different roughness scales could result in different lubrication performances. It is still unclear what the criteria are for choosing the scales of roughness used in those simulations.

In order to explore the solution to this critical problem, a point-contact elastohydrodynamic lubrication (EHL) problem is used as a standard research object. Then, inspired by the work of Venner and Lubrecht [29], a series of single-scale wavinesses is generated to represent the multiscale roughness. These single-scale wavy surfaces are used as inputs to simulate the EHL problems. The corresponding EHL performance parameters are considered a standard reference showing the responses of the EHL system to roughness components within different scales. The full film conditions have been reported in the Part I paper [1]. This paper continues the previous work and focuses on the partial film conditions where asperity contacts occur.

This article is organized as follows. First is a brief introduction to the theories and methods. More details about the models and algorithms and their validations can be found in the previous Part I paper [1]. Then, simulation conditions are introduced, and the corresponding results are discussed and analyzed.

2. Materials and Methods

2.1. Computation Model

The current research uses the same transient thermal EHL model (TEHL) as the previous Part I paper [1], where modeling details can be found. To keep the current paper complete and concise, some features of the model are provided in Supplemental Materials S1.

One point that needs to be addressed is the ability of the computation model to deal with mixed lubrication conditions. The physical model in Part II is the same as that in Part I. The numerical algorithm is the key to this model dealing with mixed lubrication. The Couette flow term at the right hand of the Reynolds equation is explicitly expressed as a function of the unknown pressure values. The unknown pressure values and their corresponding coefficients are transposed to the left hand of the Reynolds equation and combined with the unknown pressures in the Poiseuille terms. By doing so, the coefficient matrix of the discrete Reynolds equation can keep the diagonal dominant with ultrathin film thickness down to sub-nanometers. Thus, it ensures that the simulations can evaluate the mixed lubrication regime. Many researchers have used this technique [25,30,31]. The specific expressions of the discrete Reynolds equation are provided in the Supplemental Material of the Part I paper.

2.2. Wavy Surface Generation

The current research uses the same structure of wavy surfaces as the previous Part I paper [1], having three essential parameters: amplitude A, frequency Ω_x, and direction θ. Detailed information on the functions of wavy surfaces is provided in Supplemental Materials S1.

A is defined as the non-dimensional amplitude shown below,

$$A = \frac{a}{h^s_{cent}} \tag{1}$$

where a is the dimensional amplitude, h^s_{cent} represents the central film thickness with the smooth surface.

Ω_x is defined as the non-dimensional frequency shown below,

$$\Omega_x = \frac{2\pi N_w}{3} \tag{2}$$

where N_w is the number of waves in the solution domain.

2.3. Numerical Simulation Details

The codes used are the same as those in the previous Part I paper [1]. It should be noted that the validation provided in the Part I paper includes the mixed lubrication scenario. The basic parameters of the EHL simulation are also the same as those in the Part I paper. The parameters table is provided in Supplemental Materials S1 of the current paper.

The working conditions of simulations are two loads, w = 200 N and 500 N, and two speeds, u_s = 0.3 m/s and 2 m/s. These parameters result in full film conditions before incorporating the waviness. In the previous Part I paper, the highest speed is u_s = 3 m/s. The current paper reduces the highest speed to 2 m/s due to convergent difficulties dealing with the partial film regimes. The corresponding performance parameters at smooth conditions are given in Table 1.

Table 1. Performance parameters at the four smooth working conditions (without wavy surfaces).

Load, w (N)	**200**		**500**	
Speed, u_s (m/s)	**0.3**	**2**	**0.3**	**2**
Central film thickness, h^s_{cent} (μm)	0.0677	0.2494	0.0628	0.2382
Minimum film thickness, $h^s_{\min}$ (μm)	0.0181	0.1029	0.0104	0.078
Average film thickness, h^s_{mean} (μm)	0.0617	0.2285	0.0571	0.2165
Central pressure, P^s_{cent} (GPa)	1.1128	1.1194	1.5081	1.5141
Maximum pressure, $P^s_{\max}$ (GPa)	1.1128	1.1195	1.5081	1.5141
Coefficient of friction, COF^s	0.0819	0.0756	0.0882	0.0791
Maximum temperature rise, $t^s_{\max}$ (K)	317.97	328.57	321.59	337.44

The non-dimensional amplitude, A, was equal to 2, 2.3, 2.7, 3, 3.3, 3.7, 4, 4.3, 4.7, and 5. The amplitude values are much greater than those used in the Part I paper ($A \in [0.02, 0.3]$) to generate partial film conditions. The frequency values are the same as those in the Part I paper, corresponding to N_w = 2, 6, 9, 12, 16, 19, 22, 25, 29, and 32.

The wave directions used in the current work are the same as those in the Part I paper, which are $\theta = 0^\circ$ (transverse), -30°, -60°, and -90° (longitudinal). The time interval and total time steps are set to the same values as those in the previous Part I paper [1]. The simulations were run at the Center of High-Performance Computing Clusters at Tsinghua University.

The critical performance parameters were extracted, including minimum film thickness, maximum pressure, central film thickness, mean film thickness, maximum temperature rise, coefficient of friction (COF), and asperity contact ratio. They are averaged over

time, during which the transient solution is stable. The parameter fluctuations have the same period because the wavy surface circulates as time increases. Thus, it is reasonable to take the last surface movement period to calculate the averaged parameters that represent the stable transient solutions. The time steps used to take the average were set as the last surface movement period.

3. Results and Discussion

The simulated results were organized similarly to those in the previous Part I paper [1]. The ratios of parameters with and without the wavy surfaces were plotted as contour maps. The coordinate plane has a double logarithm scale for the non-dimensional frequency and amplitude. Here, only selected plots are shown in the current manuscript to ensure it remains concise. Readers who want to access all the results can go to Supplemental Materials S1.

3.1. The Influences of the Waviness Amplitude and Frequency

Results simulated with w = 200 N, u_s = 2 m/s, and $\theta = 0^\circ$ are discussed in this section to show how the amplitude and frequency affect when running into the mixed lubrication regime. Figures 1 and 2 show the eight contour maps, and Table 2 lists the corresponding range of values shown in the contour maps, rounded to three decimal places.

Table 2. The minimal and maximum performance parameter ratios with w = 200 N, u_s = 2 m/s, and $\theta = 0^\circ$.

Parameter	Min	Max
Minimum film thickness ratio, $h^w_{\min}/h^s_{\min}$	0	1.016
Central film thickness ratio, h^w_{cent}/h^s_{cent}	1.150	8.799
Average film thickness ratio, h^w_{mean}/h^s_{mean}	1.132	5.056
Maximum pressure ratio, $P^w_{\max}/P^s_{\max}$	1.242	20.808
Central pressure ratio, P^w_{cent}/P^s_{cent}	0.875	1.699
COF ratio, COF^w/COF^s	0.847	1.766
Maximum temperature rise ratio, $t^w_{\max}/t^s_{\max}$	1.007	1.680
Asperity contact ratio, W_c	0	0.900

In Figure 1a, the asperity contact ratio shows that the system runs into the partial film regime as the amplitude and frequency increase. The maximum asperity ratio is around 0.9 (Table 2), meaning severe asperity contacts. One should be aware of that many full film cases are still shown in Figure 1a, such as ($\Omega_x \approx 13$, A = 3.3) and ($\Omega_x \approx 19$, A = 3). Such results are unexpected because the waviness amplitude has been three times the central film thickness of the corresponding smooth EHL situations. As such, the simulation results shown here illustrate the power of the micro-EHL effects at the asperity scale.

Moreover, the maximum asperity ratio occurs at $\Omega_x \approx 46$ and A = 5. The corresponding amplitude value is the maximum amplitude used in this work. However, the corresponding frequency value is among the frequency range used. This phenomenon means the asperity contact ratio increases as the frequency rises to a maximum value. Then, as the frequency further increases, the asperity contact ratio decreases. This result illustrates that even in the partial film regime where asperity contacts occur, high-frequency waviness can improve the microscale EHL effects.

Figure 1b shows that the $h^w_{\min}/h^s_{\min}$ values are less than one in most cases. This result means that incorporating waviness causes a decrease in the minimal film thickness. The result is the same as the full film condition discussed in the Part I paper [1]. However, the maximum $h^w_{\min}/h^s_{\min}$ value seems greater than one (1.016, Table 2), meaning the minimum film thickness is increased when considering the designated waviness with relatively small amplitude and frequency ($\Omega_x \approx 4.2$ and A = 2). Such results were not in our previous studies within the full film regime. The frequency range is the same for the full (Part I paper) and partial film simulations (current work). The increase of minimal film thickness should

be due to the amplitudes used. The amplitudes used in the current work are between $A = 2$ and $A = 5$. The amplitude range used in our previous work is between 0.02 and 0.3. Therefore, it can be inferred that when the amplitude value is significant to a certain extent and the frequency is minor, the waviness can slightly increase the minimum film thickness.

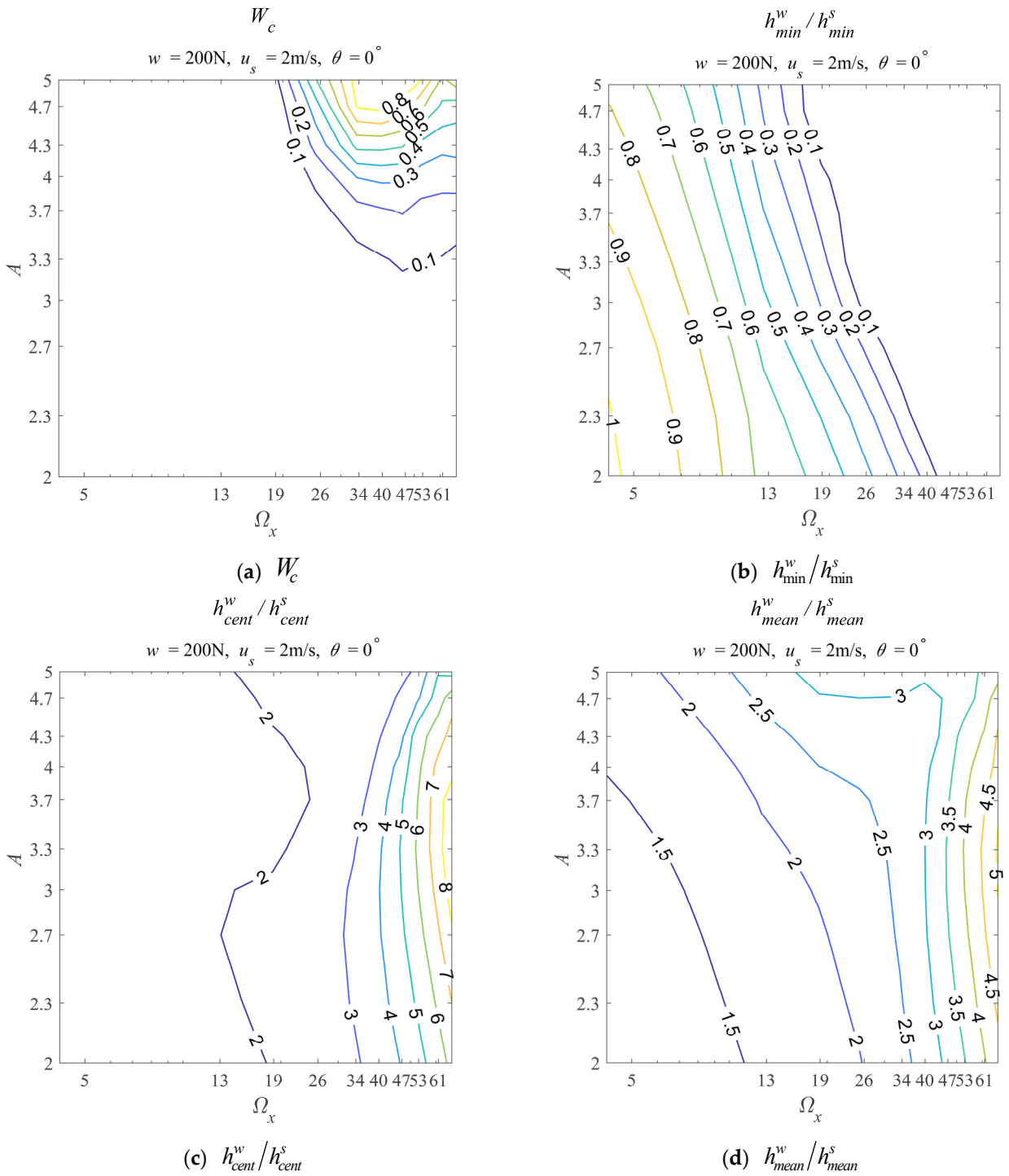

Figure 1. Contour maps with $w = 200$ N, $u_s = 2$ m/s, $\theta = 0°$, (**a**) asperity contact ratio W_c, (**b**) minimum film thickness ratio $h^w_{\min}/h^s_{\min}$, (**c**) central film thickness ratio h^w_{cent}/h^s_{cent}, and (**d**) mean film thickness ratio h^w_{mean}/h^s_{mean}.

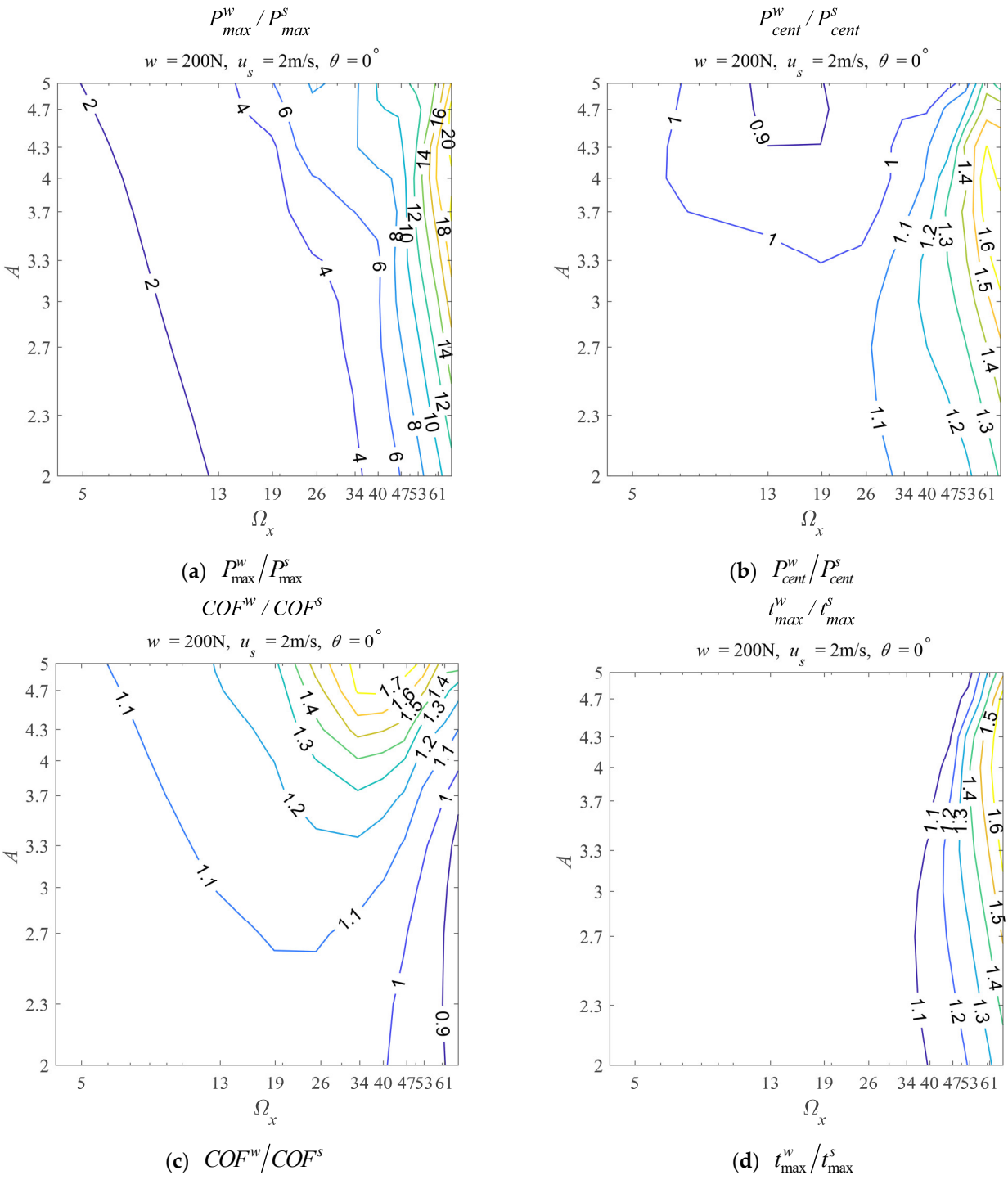

(**a**) P^w_{max}/P^s_{max} (**b**) P^w_{cent}/P^s_{cent}

(**c**) COF^w/COF^s (**d**) t^w_{max}/t^s_{max}

Figure 2. Contour maps with w = 200 N, u_s = 2 m/s, θ = 0°, (**a**) maximum pressure ratio P^w_{max}/P^s_{max}, (**b**) central pressure ratio P^w_{cent}/P^s_{cent}, (**c**) COF ratio COF^w/COF^s, and (**d**) maximum temperature rise ratio t^w_{max}/t^s_{max}.

Another point is that the minimal film thickness decreases monotonically till zero (Table 2) as the amplitude and frequency increase. This phenomenon is different from the results shown in our previous work (Part I paper). In Part I, the minimal film thickness first decreases and then increases as the frequency increases. Such a difference means the minimal film thickness will not be increased by increasing frequency when the system works in the partial film regime.

Figure 1c shows that the h^w_{cent}/h^s_{cent} ratio values are more significant than one, indicating that incorporating waviness can increase the central film thickness. Generally, the h^w_{cent}/h^s_{cent} ratio increases as the amplitude A or frequency Ω_x increases. The maximum h^w_{cent}/h^s_{cent} value in the current simulation is around 8.799 (Table 2), corresponding to $\Omega_x \approx 67$ and $A = 3.3$. The frequency value has reached the upper-frequency limit used in this work. The amplitude value is at the middle of the amplitude range. This result means that an amplitude value exists that increases the central film thickness the most. In other words, the central film thickness is more sensitive to waviness amplitude.

The contour map of the mean film thickness ratio (Figure 1d) has a similar pattern to that of the central film thickness (Figure 1c). The h^w_{mean}/h^s_{mean}ratio values are more significant than one, meaning the waviness can enhance the mean film thickness. In general, the h^w_{mean}/h^s_{mean} ratio increases as A or Ω_x increases. The maximum h^w_{mean}/h^s_{mean}value in the current simulation is around 5.056 (Table 2), corresponding to $\Omega_x \approx 67$ and $A = 3.3$. This pair of amplitude and frequency is the same as that which corresponds to the maximum h^w_{cent}/h^s_{cent}value. It is expected that the maximum h^w_{mean}/h^s_{mean} value (5.056) is smaller than the maximum h^w_{cent}/h^s_{cent} value (8.799). Moreover, a specific amplitude value still increases the mean film thickness the most, just like the situation in the central film thickness. Thus, the mean film thickness can be considered more sensitive to waviness amplitude.

When comparing the contour maps of the central and mean film thicknesses between the partial (this paper) and full (Part I paper) film conditions, the most significant difference is the amplitude and frequency values corresponding to their maxima. In our previous work, where the amplitude range is between 0.02 and 0.3, the amplitude and frequency corresponding to the maximum central and mean film thickness ratios are at the maximum frequency and amplitude used in the simulations. However, in this work ($A \in [2, 5]$), the maximum h^w_{cent}/h^s_{cent} and h^w_{mean}/h^s_{mean} values are obtained with the maximum frequency and a medium amplitude ($A = 3.3$). Such a difference illustrates that as the amplitude continuously increases, the central and mean film thickness will not monotonically increase. The central and mean film thickness will decrease when the asperity contact ratio is high enough. As for the frequency value, it is clear that within the frequency range used, the higher the frequency is, the greater the enhancement of central and mean film thickness.

In summary, when the point contact EHL system runs into the partial film regime, the waviness can increase the central and mean film thickness while decreasing the minimum film thickness in most cases. Usually, an increase in the central and mean film thickness means that the EHL effect is enhanced. Decreasing the minimum film thickness implies that although the ball is lifted, it still cannot counteract the influences of the valleys caused by waviness.

It should be highlighted that the minimal film thickness can be increased with the minimum frequencies and amplitude ($\Omega_x \approx 4.2$ and $A = 2$) used in the simulations with $w = 200$ N, $u_s = 2$ m/s, and $\theta = 0°$. Therefore, one can have a specific situation in which the central, mean, and minimum film thickness all increase by controlling the amplitude and frequency of the waviness. That is the waviness with $\Omega_x \approx 4.2$ and $A = 2$. In our previous paper [1], the recommended waviness parameters were the maximum frequency ($\Omega_x \approx 67$) and maximum amplitude ($A = 0.3$) used in the simulations for the EHL problem with $w = 200$ N, $u_s = 3$ m/s, and $\theta = 0°$. Such an opposite recommendation is due to the lubrication regime and the amplitude range considered. Therefore, one should remember that when approaching the partial film regime by increasing the waviness amplitudes, the best choice of amplitudes and frequencies to enhance the EHL effects needs to be re-examined.

Figure 2 shows the contour maps of ratios of the pressure parameters, friction coefficient, and the maximum temperature rise with and without waviness. Figure 2a illustrates that the $P^w_{\max}/P^s_{\max}$ ratios are greater than one. This result means that incorporating waviness leads to an increase in maximum pressure. When the A or Ω_x increases, the maximum pressure ratio increases. The maximum $P^w_{\max}/P^s_{\max}$ value is approximately 20.808. It occurs at the point with the maximum frequency ($\Omega_x \approx 67$) and an intermediate amplitude value

(A = 4.7), nearing the maximum amplitude used in the simulations. Such phenomena mean that the increase of the amplitude or frequency could synergistically lead to the rise of maximum pressure in most cases. Moreover, the maximum $P^w_{\max}/P^s_{\max}$value here exceeds our previous Part I paper. The reason should be that the amplitudes used here are much greater than those in the Part I paper.

If one looks at Figures 1a and 2a simultaneously, it can be found that the maximum pressure occurs when the asperity contact occurs. However, the maximum pressure and maximum asperity contact ratios have different corresponding frequencies and amplitudes. The maximum asperity ratio occurs at $\Omega_x \approx 46$ and A = 5, while the maximum $P^w_{\max}/P^s_{\max}$ value occurs at $\Omega_x \approx 67$ and A = 4.7. Generally, researchers prefer to think the larger the asperity contact ratio is, the higher the maximum contact pressure will be. Thus, such a difference challenges this common idea and suggests one should consider the asperity contact ratio and maximum pressure separately.

Furthermore, Figure 1 shows that waviness with a high frequency and significant amplitude can lead to a thicker lubricant film regarding the central and mean film thickness. At the same time, Figure 2a shows that such cases lead to more significant maximum pressure. Maximum pressure increases are usually regarded as unfavorable in an EHL problem. Therefore, one needs to comprehensively evaluate the effects of wavy surfaces on the film thickness and pressure when waviness is introduced to the EHL system.

Figure 2b illustrates the central point pressure ratios (P^w_{cent}/P^s_{cent}) with and without waviness. The P^w_{cent}/P^s_{cent} results fluctuate between 0.875 and 1.699. This range is around one and is much smaller than that of the $P^w_{\max}/P^s_{\max}$ (between 1.242 and 20.808). Moreover, the fluctuation of the P^w_{cent}/P^s_{cent} ratios is more relevant to the change in the frequencies. Such results are similar to that in the Part I paper. The central pressure value is more dominated by the maximum Hertzian contact pressure, which is a constant when the load of the EHL system is given. Therefore, whether in the full or partial film regime, the P^w_{cent}/P^s_{cent} ratio contour map is the one having less information when compared with the $P^w_{\max}/P^s_{\max}$ ratio contour map.

Figure 2c shows the ratios of the coefficient of friction with and without wavy surfaces (COF^w/COF^s). The COF^w/COF^sratios vary from 0.847 to 1.766. It is clear that the COF ratio increases first and then decreases as the frequency increases. As for the amplitude, increasing it increases the COF ratio within the simulations of the current work. Thus, the minimum COF ratio occurs at $\Omega_x \approx 67$ and A = 2.7, a waviness with a high frequency and small amplitude. The maximum COF ratio occurs at $\Omega_x \approx 40$ and A = 5. Such a specific combination of frequency and amplitude is close to parameters leading to the maximum asperity contact ratio (Figure 1a, $\Omega_x \approx 46$ and A = 5). This phenomenon indicates that the maximum COF mainly depends on the asperity contact ratio when the system works in the partial film regime.

It should be highlighted that in our Part I paper, where the amplitude is relatively small ($A \in [0.02, 0.3]$), the COF ratio decreases to smaller than one as the amplitude and frequency increase. Such a vast difference should be due to the differences in the composition of friction force between full and partial film regimes. The friction force in the full film regime is merely the viscous shear force within lubricants. In the partial film regime, the friction force comprises the lubricant's viscous shear and the solid friction between asperities. The solid friction between asperities is much greater than the viscous shear force. Therefore, once the asperity contacts are severe to a certain extent, the solid friction between them will dominate the comprehensive friction. Furthermore, it can be concluded that once the EHL system runs in the partial film regime, it would be better to have a relatively smooth surface topography to reduce the COF.

Figure 2d illustrates that the $t^w_{\max}/t^s_{\max}$ ratios are greater than one. This phenomenon means that the temperature rise in the lubricated zone is increased by incorporating wavy surfaces. The $t^w_{\max}/t^s_{\max}$ ratio seems to be more sensitive to the frequency values. As the frequency increases, the $t^w_{\max}/t^s_{\max}$ ratio increases significantly. When increasing the amplitude, the $t^w_{\max}/t^s_{\max}$ ratio slightly increases and then decreases. It is worth reminding

readers that the results in the Part I paper show that increasing the $t^w_{\max}/t^s_{\max}$ value leads to decreasing viscosity, then reducing the COF when the EHL system is within the full film regime. This relationship is still valid in the current work, although the asperity contacts occur. The maximum $t^w_{\max}/t^s_{\max}$ ratio is around 1.680 when $\Omega_x \approx 67$ and $A = 3.7$. The COF and asperity contact ratios corresponding to this specific frequency and amplitude are around 0.921 and 0.144, respectively. This result means that even when the asperity contacts occur, one can still obtain a reduction of COF by designing the amplitude and frequency of waviness to decrease the viscosity by increasing the temperature.

Considering the results in Figures 1 and 2, when the amplitude increases to initiate asperity contacts, a wavy surface with a high frequency and large amplitude can generally generate a severe asperity contact ratio, resulting in a thicker mean and central film thickness. In the meantime, the maximum pressure, COF, and temperature rise increases. Usually, a thicker lubricant film is considered a good point, but the increase of maximum pressure or maximum temperature rise is considered unfavorable. These results further suggest that one needs to comprehensively evaluate these pros and cons to decide whether waviness benefits their studies.

3.2. The Influence of the Wave Direction

The influence of wave direction is discussed based on the simulations with load equaling 200 N and speed equalling 2 m/s. In order to compare the results directly with different wave directions in one graph, the simulated data were processed as follows. For each contour map, two cross lines were extracted. One crossline is the data whose amplitude is fixed to $A = 3.7$. Another crossline is the data whose frequency is fixed to $\Omega_x \approx 39.8$ ($N_w = 19$). Then, the extracted lines were organized by the different kinds of performance parameters. In every single graph, there are four curves corresponding to the four directions: $\theta = 0°$, $-30°$, $-60°$, and $-90°$. Figure 3 shows all the sub-figures, sixteen in total. Indices (a) to (h) represent the eight performance parameters, where '1' and '2' represent the results of $N_w = 19$ and $A = 0.09$, respectively.

Figure 3a.1 illustrates that the asperity contact ratio increases as the amplitude increases for most cases. The increase trends are similar for the wave directions of $0°$, $-30°$, and $-60°$. That is, when the amplitude is relatively small, the asperity contact ratio is zero, meaning no asperity contact. However, for the longitudinal ($-90°$) waviness, there are significant asperity contacts even with the minimal amplitude used in the current simulations. Such differences between longitudinal and other directions of waviness also appeared in our previous Part I paper.

Figure 3a.2 shows that all the wave directions have similar trends of asperity contact ratio as the frequency increases. The asperity contact ratio first increases from zero to a maximum value and then decreases as the frequency increases. This phenomenon means that specific waviness frequencies may weaken the micro-EHL effects most in the mixed lubrication regime, resulting in the maximum asperity contact ratio. Moreover, considering the transformation of transverse ($0°$) waviness to longitudinal waviness ($-90°$), Figure 3a.1,a.2 clearly show that the asperity ratios generally increase along with such a process.

All the $h^w_{\min}/h^s_{\min}$ ratios in Figure 3b.1,b.2 are less than one. This phenomenon means that incorporating waviness decreases the minimum film thickness. Moreover, as the amplitude or frequency increases, the EHL system works in the partial film regime; thus, the minimum film thickness is gradually reduced to zero, indicating that asperity contacts are occurring. The amplitude or frequency value corresponding to the zero minimum film thickness decreases as the wave direction changes from $0°$ to $-90°$ (transverse to longitudinal). This result again shows that the transverse waviness can enhance the EHL effects the most, while the longitudinal waviness has little positive effect on the EHL effects. This point is consistent with the results reported in our previous Part I paper [1].

Figure 3c.1,c.2 show the h^w_{cent}/h^s_{cent} ratios. It is evident that the longitudinal waviness ($\theta = -90°$) results in a different trend of the central film thickness ratios compared to wave

directions of $\theta = 0°$, $-30°$, and $-60°$. In Figure 3c.1, when $\theta = 0°$, $-30°$, and $-60°$, the central film thickness ratios are more significant than one and decrease as the amplitude increases. When the wave direction is longitudinal ($\theta = -90°$), the central film thickness is zero and does not change as the amplitude changes. In Figure 3c.2, when $\theta = 0°$, $-30°$, and $-60°$, the central film thickness ratios are almost greater than one and follow an increasing trend as the frequency increases. When $\theta = -90°$, a decreasing trend is observed as the frequency increases. Moreover, as the wave directions turn from $\theta = 0°$ to $\theta = -30°$, the h^w_{cent}/h^s_{cent} ratios decrease. Thus, it can be concluded that turning the waviness from transverse to longitudinal usually decreases the h^w_{cent}/h^s_{cent} ratio.

Figure 3d.1,d.2 show the mean film thickness ratios. They have similar patterns to the central film thickness ratios shown in Figure 3c.1,c.2. In Figure 3d.1, when $\theta = 0°$, $-30°$, and $-60°$, the mean film thickness ratios are more significant than one, while $\theta = -90°$, the mean film thickness ratios are smaller than one. Moreover, when $\theta = 0°$, $-30°$, the mean film thickness ratios increase as the amplitude increases. In comparison, the mean film thickness ratios decrease as the amplitude increases when θ = -60°, $-90°$. As shown in Figure 3d.2, when the frequency is not greater than 19, the four directions of waviness correspond to mean film thickness ratios greater than one. The h^w_{mean}/h^s_{mean} ratios increase as the frequency increases. When the frequency is greater than 19, the mean film thickness ratios still increase as the frequency increases for $\theta = 0°$, $-30°$. While for $\theta = -60°$, $-90°$, the mean film thickness decreases rapidly as the frequency increases to around 34. Then, the mean film thickness ratio increases again for $\theta = -60°$ and decreases slowly for $\theta = -90°$. Furthermore, the mean film thickness ratio can be smaller than one when $\theta = -90°$. These results mean that the h^w_{mean}/h^s_{mean} ratios decrease as the wave directions turn from transverse to longitudinal. Moreover, the effects of amplitude and frequency on the mean film thickness ratios show different trends as the wave directions turn to longitudinal.

Based on the discussion in Figure 3a–d, it is readily known that turning the waviness from a transverse to a longitudinal direction usually decreases the lubricant film thickness. This point is the same as that drawn from the simulations within the full film regime. The reasons behind such phenomena are also the same as those discussed in the previous Part I paper [1]. When the wave direction is turned from transverse to longitudinal, the equivalent frequency decreases in the direction of the relative motion (X-direction), decreasing the EHL effects regarding the film thickness.

Furthermore, comparing the results regarding the film thickness in this paper (corresponding to partial film regime) with those in our previous Part I paper [1] (corresponding to full film regime), it can be found that the longitudinal waviness has more significant effects when the EHL system works in the partial film regime.

Figure 3e.1,e.2 show that the $P^w_{\max}/P^s_{\max}$ ratios are significantly affected by the alterations in the wave directions. This phenomenon differs from that shown in the Part I paper, where the maximum pressure ratios are almost unaffected by wave directions except $\theta = -90°$. The maximum pressure ratios increase as the amplitude increases for most cases, as shown in Figure 3e.1. As the wave direction changes from 0° to $-90°$, the growth rate of such an increasing trend first increases and then decreases. The fastest case in the current simulations is the waviness, whose direction is $-60°$.

Figure 3e.2 shows similar trends, but the growth rate is also sensitive to the frequency of waviness. When the frequency is no greater than 13, the maximum pressure ratios increase as the frequency increases. Moreover, the corresponding growth rate is almost the same. When the frequency further increases to around 47, the maximum pressure ratios increase at a different rate corresponding to wave directions. The wave direction of $-60°$ is still the fastest-increasing case. A sharp peak appears for the longitudinal waviness. As the frequency increases to the maximum value used in the current simulations, the increase rate corresponding to the transverse waviness gradually exceeds other wave directions. Overall, combining Figure 3e.1,e.2, the maximum pressure increase is the slightest when the wave direction is longitudinal.

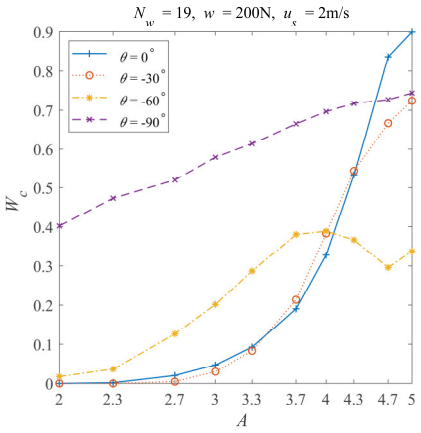

(a.1)

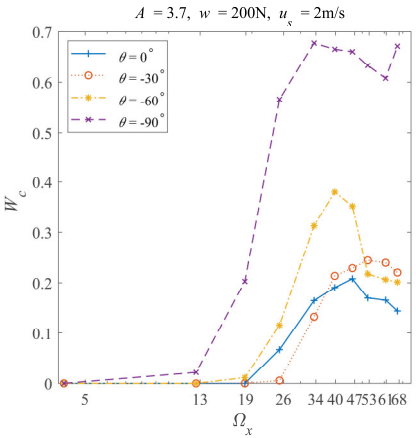

(a.2)

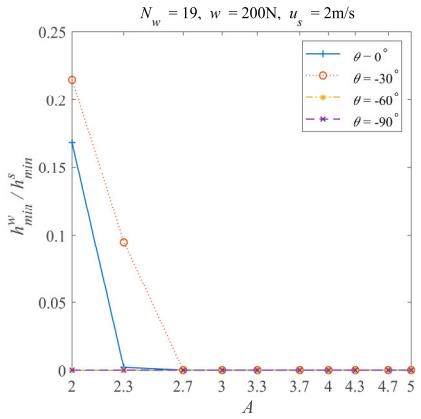

(b.1)

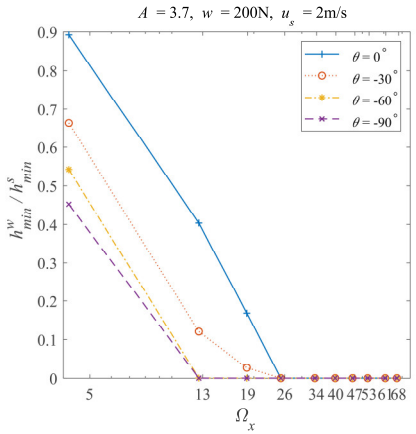

(b.2)

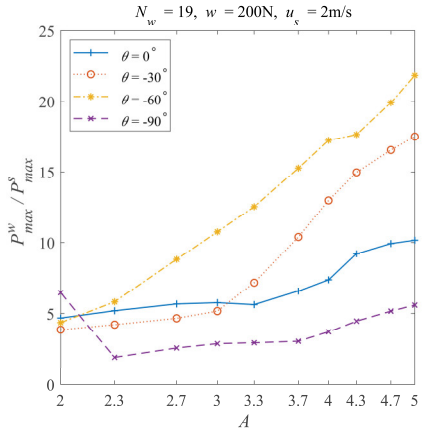

(e.1)

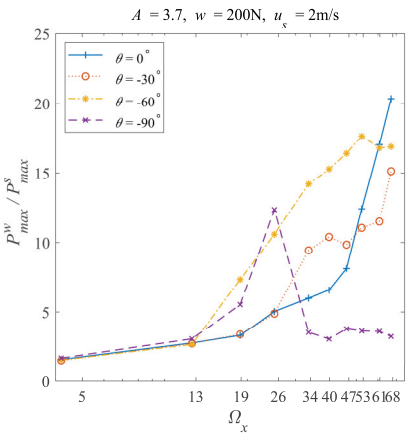

(e.2)

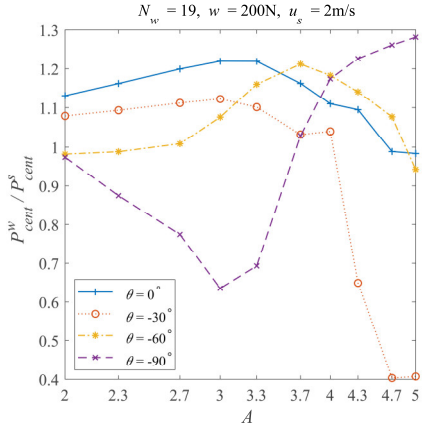

(f.1)

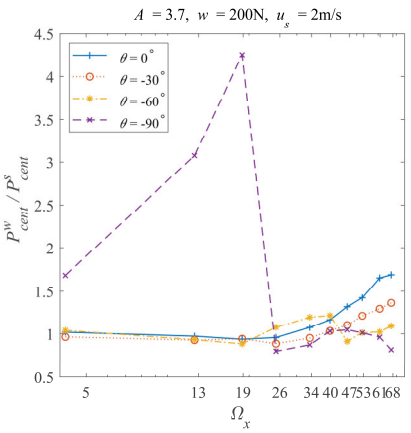

(f.2)

Figure 3. *Cont.*

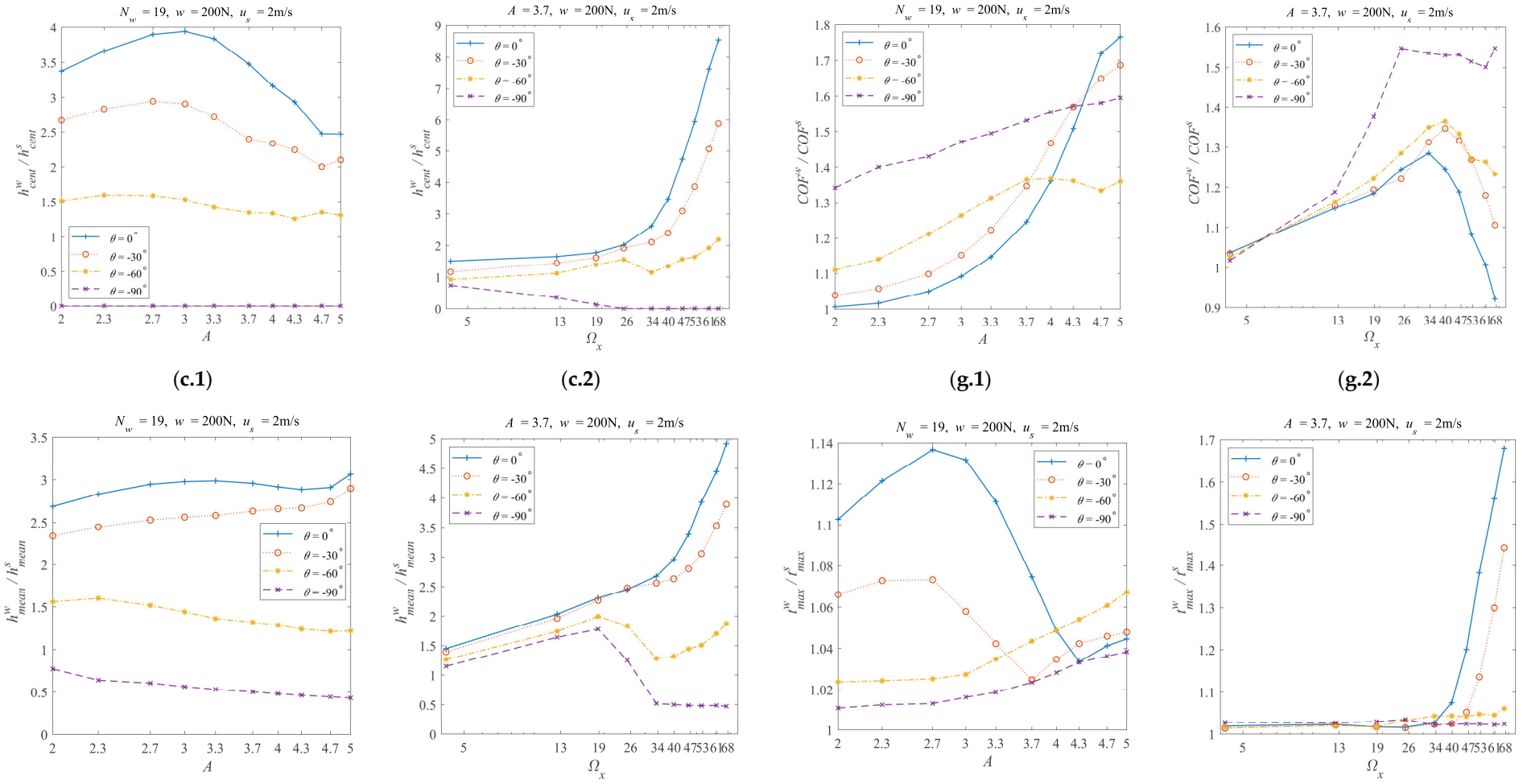

Figure 3. Performance parameters with $w = 200$ N, $u_s = 2$ m/s, $\theta = 0°$, $-30°$, $-60°$, and $-90°$. Here, a to h are (**a**) W_c, (**b**) $h^w_{\min}/h^s_{\min}$, (**c**) h^w_{cent}/h^s_{cent}, (**d**) h^w_{mean}/h^s_{mean}, (**e**) $P^w_{\max}/P^s_{\max}$, (**f**) P^w_{cent}/P^s_{cent}, (**g**) COF^w/COF^s, (**h**) $t^w_{\max}/t^s_{\max}$. '**1**' indicates the results of fixed $N_w = 19$ ($\Omega_x \approx 39.8$), and '**2**' indicates the results of fixed $A = 3.7$.

Figure 3f.1 shows that the P^w_{cent}/P^s_{cent} ratios vary differently as the amplitude increases when the wave direction changes. The central pressure ratio values can be greater or less than one. When $\theta = 0°, -60°$, the variation range of the central pressure ratios is relatively small compared with that corresponding to $\theta = -30°, -90°$. The minimum central pressure ratio is around 0.4 when the wave direction is $-30°$ and the amplitude reaches 4.7. The maximum central pressure ratio is close to 1.3 when the wave direction is $-30°$ and the amplitude is 5. In Figure 3f.2, the P^w_{cent}/P^s_{cent} ratios are around one and have slight differences when $\theta = 0°, -30°$, and $-60°$. The central pressure ratio sharply peaks as the frequency increases when the wave direction is longitudinal. The maximum value is greater than 4 when the frequency is around 19. These phenomena illustrate that the central pressure is more sensitive to longitudinal waviness than other wave directions.

Figure 3g.1,g.2 provide the COF^w/COF^s ratios. It should be highlighted that the patterns are largely the same as those shown in Figure 3a.1,a.2, representing the asperity contact ratios. This phenomenon is because the simulated EHL system works in the partial regime. When asperity contacts occur, the friction force between asperities is much greater than the viscous friction. The summation of asperity friction force and viscous friction equals the total friction force. Thus, the COF ratios show the same patterns as the asperity contact ratios. Another point to address is that the COF ratios can be smaller than one, meaning a friction reduction by incorporating waviness when the amplitude and frequency of waviness are appropriately designed (e.g., $A = 3.7$, $\Omega_x \approx 67$, $\theta = 0°$ in Figure 3g.2). It should be noted that the COF is hardly decreased by longitudinal waviness.

Figure 3h.1 illustrates that the $t^w_{\max}/t^s_{\max}$ ratios fluctuate as the amplitude increases. When $\theta = 0°$ or $-30°$, the maximum temperature rise ratio first slowly increases, rapidly decreases, and then increases again as the amplitude increases. When $\theta = -60°$ or $-90°$, the maximum temperature rise ratio slowly increases as the amplitude increases. These results suggest that the variation of the maximum temperature rise ratio corresponding to amplitude is sensitive to the wave directions. In Figure 3h.2, the results are pretty different from those in Figure 3h.1. The maximum temperature rise ratio for all four wave directions does not vary much when the frequency value is no greater than 34. As the frequency further increases, the maximum temperature rise ratio corresponding to the wave direction of $0°$ first increases rapidly, then the $-30°$ and $-60°$ waviness. The $-90°$ waviness does not significantly increase the maximum temperature rise ratio. These phenomena prove that among the wave directions simulated, the longitudinal waviness is the one decreasing the maximum temperature rise most.

According to the discussions above, the waviness with $\theta = 0°, -30°$, and $-60°$ results in more similar results than those with longitudinal waviness ($\theta = -90°$). Thus, it can be concluded that waviness turning to the longitudinal direction usually increases the asperity contact ratio, decreases the film thickness, and increases the COF. At the same time, the maximum pressure increases, and the maximum temperature rise decreases as the wave direction changes from $0°$ to $-60°$. The central pressure is relatively slightly affected by changing the wave directions. The increase in COF is due to the rise of asperity contact ratios, which dominate in generating friction force. In our previous Part I paper, the COF reduces when the transverse waviness turns to longitudinal waviness because the system works in a full film regime.

The longitudinal ($\theta = -90°$) waviness is expected to result in different patterns than other wave directions. In our previous Part I paper, such phenomena have been thoroughly analyzed. This is because the initial surface geometry is not changed in the relative motion direction by the longitudinal waviness, meaning little additional EHL effect as the longitudinal waviness passes the Hertzian contact domain. Therefore, the current paper does not discuss the results separately with longitudinal waviness. However, all the contour maps can be found in Supplemental Materials S1 for readers' convenience.

3.3. The Influences of the Load and Speed

Based on Section 3.2, the transverse waviness ($\theta = 0°$) generates the most significant additional EHL effects in most cases. Thus, the results simulated with transverse waviness are used to analyze the impact of the different load and speed combinations.

In the current work, four combinations of loads and speeds were simulated. They are indexed based on the severity of the corresponding EHL situations. That is, the thinner the film thickness is, the harsher the working conditions are. Referring to Table 1, the order of the four combinations is: i: (w = 500 N, u_s = 0.3 m/s), ii: (w = 200 N, u_s = 0.3 m/s), iii: (w = 500 N, u_s = 2 m/s), and iv: (w = 200 N, u_s = 2 m/s), which is from harsh to mild. Two cross lines, the same as those extracted in Section 3.2, were also used. Figure 4 shows the graphs. Indices (a) to (h) represent the eight performance parameters, where '1' and '2' represent the results of Nw = 19 and A = 0.09, respectively.

Figure 4a.1,a.2 show that the asperity contact ratio W_c is significantly affected by working conditions. As the working condition changes from harsh to mild (i to iv), the asperity contact ratio increases in general. Such phenomena suggest that mild working conditions result in relatively severe asperity contacts. To understand this counterintuitive result, the definition of amplitude and frequency should be considered. The non-dimensional amplitude and frequency are defined based on the central film thickness and the size of the solution domain corresponding to the smooth EHL. Thus, although the non-dimensional amplitude and frequency shown in Figure 4a.1,a.2 are the same for the four working conditions, the dimensional amplitude and frequency are very different.

For example, in mild working conditions, such as working condition iv, the film thickness is thicker than other harsher working conditions, showing more significant EHL effects. However, according to Equation (1), the same non-dimensional amplitude A results in a much greater dimensional amplitude for working condition iv than for other harsher working conditions. Such a difference in the dimensional wavy amplitude can neutralize the significant EHL effects of mild working conditions and result in relatively severe asperity contacts compared to harsh working conditions.

Figure 4b.1,b.2 show the minimal film thickness ratio, $h^w_{\min}/h^s_{\min}$. It is significantly influenced by working conditions as well. When the working condition changes from harsh to mild (i to iv), the minimal film thickness ratio decreases from greater to smaller than one in general. This result indicates that the minimum film thickness can be increased by incorporating waviness when working in harsh conditions. When the working conditions become mild (i to iv), the wavy surface gradually decreases the minimum film thickness. Figure 4c,d further show that the central film thickness ratio, h^w_{cent}/h^s_{cent}, and mean film thickness ratio, h^w_{mean}/h^s_{mean}, show an increasing trend when the working condition turns from harsh (i) to mild (iv).

Figure 4e,f illustrate the effects of the working conditions on the maximum pressure ratio, $P^w_{\max}/P^s_{\max}$, and the central pressure ratio, P^w_{cent}/P^s_{cent}. It shows that as the working conditions become mild, the maximum and central pressure ratios are increased in most cases. It should be noted again that incorporating waviness increases the maximum pressure no matter which working condition is used. As for the central pressure, decreasing it using specific waviness is possible.

Figure 4g.1,g.2 show that the waviness affects the COF more significantly at the mildest condition among the four working conditions (condition iv: w = 200 N, u_s = 2 m/s). Another point is that the COF can be reduced by incorporating waviness with specific amplitudes and frequencies, regardless of the working conditions used. On the other hand, adjusting the amplitudes and waviness can increase the COF. One should carefully choose the amplitude and frequency of waviness that satisfies their purposes.

Figure 4h.1,h.2 indicate that the speed value significantly affects the maximum temperature rise. The maximum temperature rise ratio changes considerably as the amplitude or frequency changes with a higher speed (u_s = 2 m/s, working conditions iii and iv). This phenomenon is easy to understand because the rise in temperature is mainly caused by the shear heat, which is almost proportional to speed.

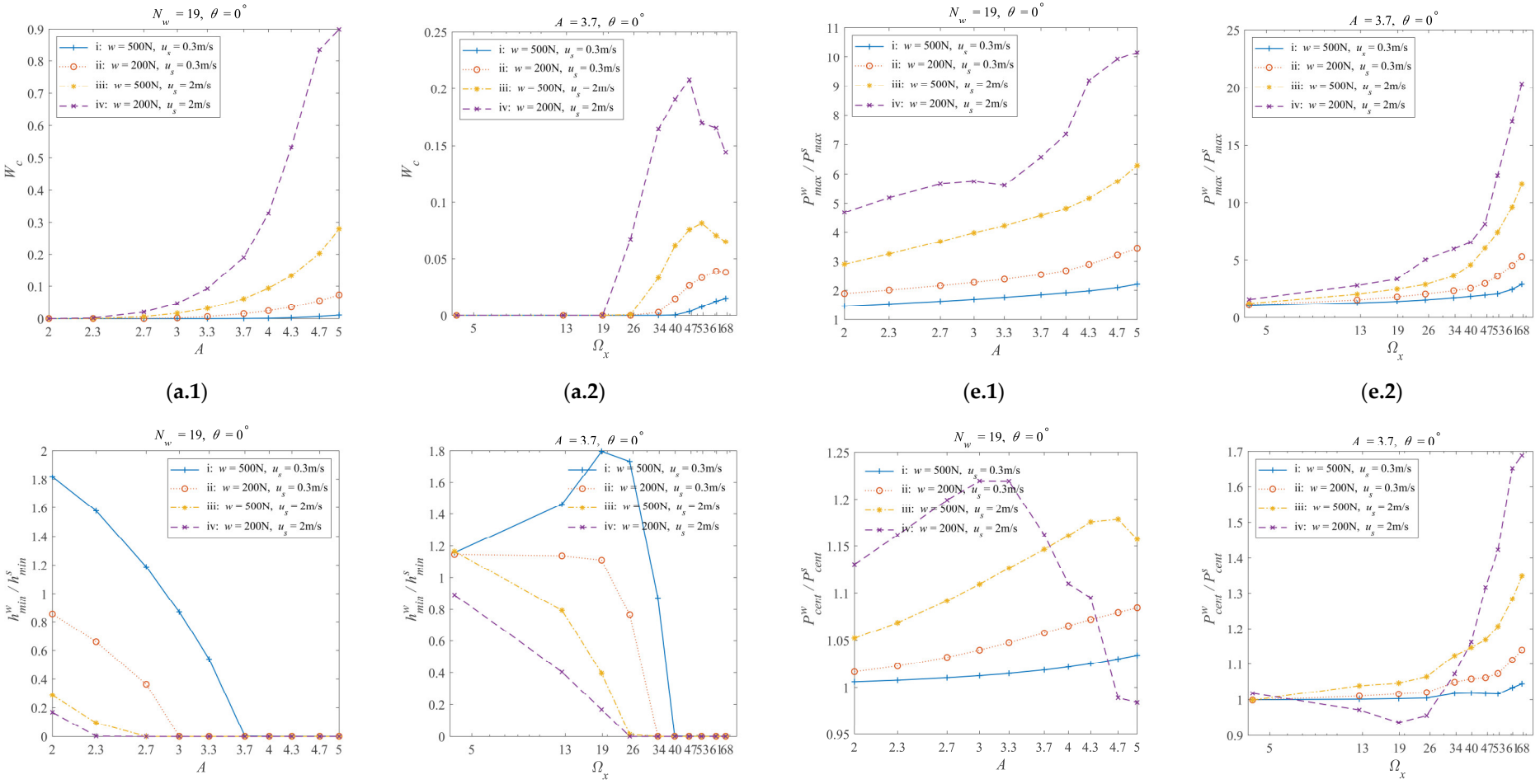

Figure 4. *Cont.*

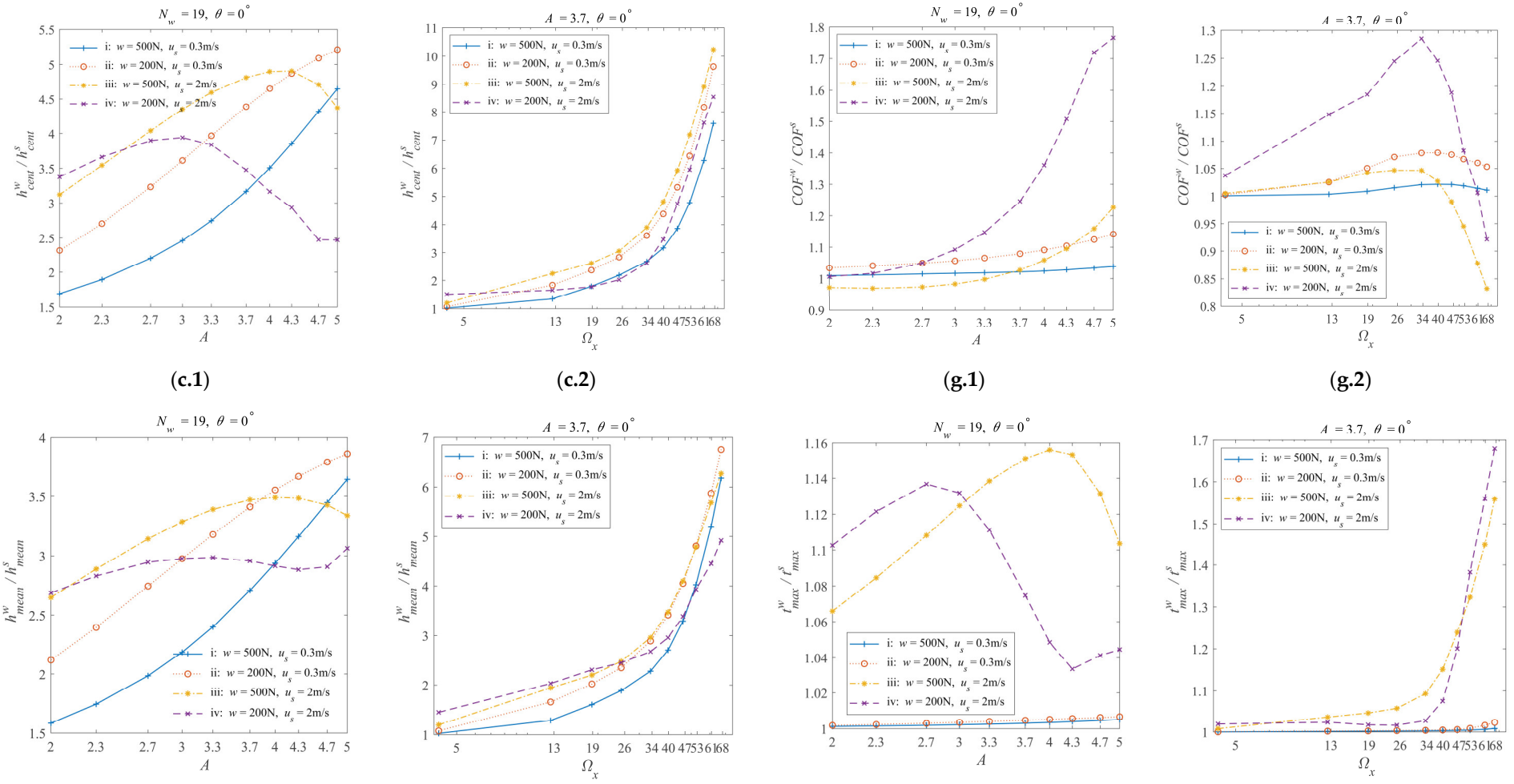

Figure 4. Performance parameters with $\theta = 0°$, w = 200 N, 500 N, u_s = 0.3 m/s, 2 m/s. Indices a to h are (**a**) W_c, (**b**) $h^w_{\min}/h^s_{\min}$, (**c**) h^w_{cent}/h^s_{cent}, (**d**) h^w_{mean}/h^s_{mean}, (**e**) $P^w_{\max}/P^s_{\max}$, (**f**) P^w_{cent}/P^s_{cent}, (**g**) COF^w/COF^s, (**h**) $t^w_{\max}/t^s_{\max}$. '**1**' indicates the results of fixed N_w = 19 ($\Omega_x \approx 39.8$), and '**2**' indicates the results of fixed A = 0.09.

In summary, mild working conditions can result in more significant influences on the EHL performance when wavy surfaces are incorporated. Such trends are the same as those in the previous Part I paper, considering only the full film lubrication regime. Moreover, the non-dimensional amplitude and frequency values are determined by the structural parameters of the EHL problem with a smooth surface. By doing so, the non-dimensional waviness is automatically adjusted according to the scale of the EHL problem. Based on the simulated results above, it is evident that although the same non-dimensional waviness is used, the results vary from different working conditions. These results reveal that the EHL system has the nature of nonlinearity.

Furthermore, two points should be addressed. First, incorporating waviness could increase the minimum film thickness under harsh working conditions. Second, the COF and maximum temperature rise results are more closely related to speed than load because the speed directly affects the shear stress.

3.4. Further Remarks on the Contour Maps

The performance parameters must be considered as a series of dependent systems when characterizing the EHL problems. Based on the results discussed, generally, incorporating waviness that enforces the system works in the partial film regime increases the asperity contact ratio and decreases the minimum film thickness. At the same time, the central and mean film thickness values are increased. In most cases simulated in the current work, the maximum pressure, COF, and maximum temperature rise values increase. It should be highlighted that the minimum film thickness and COF can be decreased simultaneously with specific combinations of waviness parameters (amplitude A, frequency Ω_x, and direction θ), even in the partial film lubrication regime. However, the maximum pressure and maximum temperature rise values, at the same time, still increase.

Another point that needs to be noted is that incorporating waviness benefits the EHL system when it has harsh working conditions. Therefore, the influences on different performance parameters must be balanced if one considers using waviness to improve the EHL system working in the partial film regime. The other important point is combining the current simulation results with those in our previous Paper I to make a series of contour maps covering a more comprehensive lubrication regime and amplitude range.

4. Conclusions

This paper is a continuity work of the previous Part I paper [1]. It studies the responses of a typical point-contact elastohydrodynamic lubrication (EHL) problem to multiscale roughness that is mimicked by artificially generated waviness with different amplitudes, frequencies, and directions. More specifically, it focuses on the partial film lubrication regime. A series of working conditions were considered in simulations as well. The corresponding performance parameters were discussed in detail. The main conclusions are as follows:

1. When the amplitude increases to initiate asperity contacts, waviness with a high frequency and large amplitude can generate severe asperity contact ratio, a thicker lubricant film regarding the mean and central film thickness, with a higher maximum pressure, a greater COF, and a higher temperature rise. The minimum film thickness decreases in most cases but still can increase with specific combinations of waviness parameters.
2. The waviness turning to longitudinal (-90°) increases the asperity contact ratio, decreases the film thickness, and increases the COF. In the meantime, the maximum pressure increases, and the maximum temperature rise decreases as the wave direction turns from 0° to -60°. The central pressure is relatively slightly affected by changing the wave directions. The increase in COF is due to the rise of asperity contact ratios, which dominate in generating friction force.
3. Mild working conditions can result in more significant influences on the EHL performance when wavy surfaces are incorporated. The minimum film thickness can

be increased, and the COF can be decreased when the working condition is harsh, even in the partial film lubrication regime. The COF and maximum temperature rise results are more closely related to speed than load.

4. The influences on different performance parameters must be balanced if one considers using waviness to improve the EHL system working in the partial film regime.

Furthermore, combining this paper and the previous Part I paper, one can make a series of contour maps covering a more comprehensive lubrication regime and amplitude range, which could be a helpful reference for researchers to understand the effects of waviness on point EHL systems comprehensively. Moreover, experimental work on different waviness is planned soon, which will further validate these findings based on simulations.

Supplementary Materials: The following supporting information can be downloaded at: https://www.mdpi.com/article/10.3390/lubricants12060190/s1, 'Supplemental Material S1.zip, including the files: 'Additional Material for Methods.pdf', 'Contour plots.docx', 'ReadMe.pdf', and 'Results_all_X_partial.mat'.

Author Contributions: Conceptualization, Y.W. and Y.L.; Funding acquisition, Y.W. and Y.L.; Methodology, Y.W. and Y.L.; Project administration, Y.W. and Y.L.; Software, Y.W.; Supervision, Y.L.; Validation, Y.W.; Writing—original draft, Y.W.; Writing—review and editing, Y.W. and Y.L. All authors have read and agreed to the published version of the manuscript.

Funding: This research was funded by the Shenzhen Science and Technology Innovation Commission, grant number GXWD20231129144211001, Shenzhen Talent Program, grant number, SZTP4202301629, and Harbin Institute of Technology, Shenzhen, grant number 20220068. National Natural Science Foundation of China, grant number 51975315.

Data Availability Statement: The data that support the findings of this study are available from the corresponding author, Y.L., upon reasonable request.

Acknowledgments: Supported by Center of High-Performance Computing, Tsinghua University.

Conflicts of Interest: The authors declare no conflicts of interest. The funders had no role in the design of the study; in the collection, analyses, or interpretation of data; in the writing of the manuscript; or in the decision to publish the results.

Nomenclature

a	dimensional amplitude of the waviness, m
A	non-dimensional amplitude of waviness
b	radius of the Hertzian contact zone, m
M, N	number of grids in the X and Y directions, respectively
COF^w/COF^s	ratio of the COF with and without waviness
$h^w_{\min}/h^s_{\min}$	ratio of the minimum film thickness with and without waviness
h^w_{cent}/h^s_{cent}	ratio of the central film thickness with and without waviness
h^w_{mean}/h^s_{mean}	ratio of the mean film thickness with and without waviness
N_T	time step for the termination of the simulation
N_w	number of waves in the solution domain
$P^w_{\max}/P^s_{\max}$	ratio of the maximum pressure with and without waviness
P^w_{cent}/P^s_{cent}	ratio of the central pressure with and without waviness
r_θ	waviness in direction θ, m
$t^w_{\max}/t^s_{\max}$	ratio of the maximum temperature rise with and without waviness
$\bar{t}$	non-dimensional time in the simulation
$\Delta\bar{t}$	non-dimensional time interval of the simulation
u_1	velocity of the smooth surface, m/s
u_2	velocity of the waviness, m/s
u_s	sum of u_1 and u_2, m/s
U	non-dimensional speed
w	load, N
W_c	asperity contact ratio
X_s, X_e	non-dimensional start and end coordinates of the solution domain in the X direction

Y_s, Y_e	non-dimensional start and end coordinates of the solution domain in the Y direction
X_{s_l}, Y_{s_l}	non-dimensional start of waviness at $\bar{t} = 0$ with the wave direction θ
α	viscosity–pressure coefficient in the Barus viscosity law, Pa^{-1}
θ	wave direction, degree
Λ_x	non-dimensional wavelength of the waviness
Ω_x	non-dimensional frequency of the waviness

References

1. Wang, Y.; Li, C.; Du, J.; Morina, A. Understanding the Influences of Multiscale Waviness on the Elastohydrodynamic Lubrication Performance, Part I: The Full-Film Condition. *Lubricants* **2022**, *10*, 368. [CrossRef]
2. Vakis, A.I.; Yastrebov, V.A.; Scheibert, J.; Nicola, L.; Dini, D.; Minfray, C.; Almqvist, A.; Paggi, M.; Lee, S.; Limbert, G.; et al. Modeling and simulation in tribology across scales: An overview. *Tribol. Int.* **2018**, *125*, 169–199. [CrossRef]
3. Archard, J.F. Elastic deformation and the laws of friction. *Proc. R. Soc. Lond. Ser. A Math. Phys. Sci.* **1957**, *243*, 190–205.
4. Sayles, R.S.; Thomas, T.R. Surface topography as a nonstationary random process. *Nature* **1978**, *271*, 431–434. [CrossRef]
5. Mandelbrot, B.B. *The Fractal Geometry of Nature*; W. H. Freeman: New York, NY, USA, 1983; Volume 173.
6. Majumdar, A.; Tien, C.L. Fractal characterization and simulation of rough surfaces. *Wear* **1990**, *136*, 313–327. [CrossRef]
7. Majumdar, A.; Bhushan, B. Fractal Model of Elastic-Plastic Contact Between Rough Surfaces. *J. Tribol.* **1991**, *113*, 1–11. [CrossRef]
8. Bhushan, B.; Majumdar, A. Elastic-plastic contact model for bifractal surfaces. *Wear* **1992**, *153*, 53–64. [CrossRef]
9. Persson, B.N.J. Theory of rubber friction and contact mechanics. *J. Chem. Phys.* **2001**, *115*, 3840–3861. [CrossRef]
10. Müser, M.H.; Dapp, W.B.; Bugnicort, R.; Sainsot, P.; Lesaffre, N.; Lubrecht, T.A.; Persson, B.N.J.; Harris, K.; Bennett, A.; Schulze, K.; et al. Meeting the Contact-Mechanics Challenge. *Tribol. Lett.* **2017**, *65*, 118. [CrossRef]
11. Persson, B.N.J.; Albohr, O.; Tartaglino, U.; Volokitin, A.I.; Tosatti, E. On the nature of surface roughness with application to contact mechanics, sealing, rubber friction and adhesion. *J. Phys. Condens. Matter* **2004**, *17*, R1–R62. [CrossRef]
12. Majumdar, A.; Tien, C.L. Fractal network model for contact conductance. *J. Heat Transf.* **1991**, *113*, 516–525. [CrossRef]
13. Barber, J.R. Bounds on the electrical resistance between contacting elastic rough bodies. *Proc. R. Soc. Lond. Ser. A Math. Phys. Eng. Sci.* **2003**, *459*, 53–66. [CrossRef]
14. Longuet-Higgins, M.S.; Deacon, G.E.R. Statistical properties of an isotropic random surface. *Philos. Trans. R. Soc. Lond. Ser. A Math. Phys. Sci.* **1957**, *250*, 157–174. [CrossRef]
15. Nayak, P.R. Random process model of rough surfaces. *J. Lubr. Technol.* **1971**, *93*, 398–407. [CrossRef]
16. Patir, N.; Cheng, H.S. Average flow model for determining effects of 3-dimensional roughness on partial hydrodynamic lubrication. *J. Lubr. Technol.-Trans. ASME* **1978**, *100*, 12–17. [CrossRef]
17. Patir, N.; Cheng, H.S. Application of average flow model to lubrication between rough sliding surfaces. *J. Lubr. Technol.-Trans. ASME* **1979**, *101*, 220–230. [CrossRef]
18. Patir, N.; Cheng, H.S. Effect of Surface Roughness Orientation on the Central Film Thickness in EHD Contacts. In *Proceedings of the 5th Leeds-Lyon Symposium on Tribology*; Dowson, D., Ed.; Institution of Mechanical Engineers: London, UK, 1979; pp. 15–21.
19. Zhu, D.; Ai, X.L. Point contact EHL based on optically measured three-dimensional rough surfaces. *J. Tribol.-Trans. Asme* **1997**, *119*, 375–384. [CrossRef]
20. Minet, C.; Brunetiere, N.; Tournerie, B. Mixed lubrication modelling in mechanical face seals. *Proc. Stle/Asme Int. Jt. Tribol. Conf.* **2008**, *43369*, 477–479.
21. Ren, N.; Zhu, D.; Chen, W.W.; Liu, Y.; Wang, Q.J. A Three-Dimensional Deterministic Model for Rough Surface Line-Contact EHL Problems. *J. Tribol.-Trans. Asme* **2009**, *131*, 011501. [CrossRef]
22. Demirci, I.; Mezghani, S.; Yousfi, M.; El Mansori, M. Multiscale Analysis of the Roughness Effect on Lubricated Rough Contact. *J. Tribol.* **2013**, *136*, 011501. [CrossRef]
23. Lorentz, B.; Albers, A. A numerical model for mixed lubrication taking into account surface topography, tangential adhesion effects and plastic deformations. *Tribol. Int.* **2013**, *59*, 259–266. [CrossRef]
24. Zhu, D.; Wang, Q.J. Effect of Roughness Orientation on the Elastohydrodynamic Lubrication Film Thickness. *J. Tribol.-Trans. Asme* **2013**, *135*, 031501. [CrossRef]
25. Zhu, D.; Wang, J.X.; Wang, Q.J. On the Stribeck Curves for Lubricated Counterformal Contacts of Rough Surfaces. *J. Tribol.-Trans. Asme* **2015**, *137*, 021501. [CrossRef]
26. Zhang, X.; Xu, Y.; Jackson, R.L. A mixed lubrication analysis of a thrust bearing with fractal rough surfaces. *Proc. Inst. Mech. Eng. Part J J. Eng. Tribol.* **2019**, *234*, 608–621. [CrossRef]
27. Li, L.; Yang, J. Surface roughness effects on point contact elastohydrodynamic lubrication in linear rolling guide with fractal surface topographies. *Ind. Lubr. Tribol.* **2018**, *70*, 589–598. [CrossRef]
28. Pei, J.; Han, X.; Tao, Y.; Feng, S. Mixed elastohydrodynamic lubrication analysis of line contact with Non-Gaussian surface roughness. *Tribol. Int.* **2020**, *151*, 106449. [CrossRef]
29. Venner, C.H.; Lubrecht, A.A. An Engineering Tool for the Quantitative Prediction of General Roughness Deformation in EHL Contacts Based on Harmonic Waviness Attenuation. *Proc. Inst. Mech. Eng. Part J J. Eng. Tribol.* **2005**, *219*, 303–312. [CrossRef]

30. He, T.; Zhu, D.; Wang, J.; Jane Wang, Q. Experimental and Numerical Investigations of the Stribeck Curves for Lubricated Counterformal Contacts. *J. Tribol.* **2016**, *139*, 021505. [CrossRef]
31. Wang, W.Z.; Hu, Y.Z.; Liu, Y.C.; Zhu, D. Solution agreement between dry contacts and lubrication system at ultra-low speed. *Proc. Inst. Mech. Eng. Part J J. Eng. Tribol.* **2010**, *224*, 1049–1060. [CrossRef]